

Investigation of the Influence of Skewed Slots and Demagnetization Effects to Line Start Permanent Magnet Assistance Synchronous Reluctance Motors

Tien Ho Manh

University of Transport and Communications, Vietnam
hotien.ktd@utc.edu.vn

Dinh Bui Minh

School of Electrical and Electronic Engineering, Hanoi University of Science and Technology, Vietnam
dinh.buiminh@hust.edu.vn

Tu Pham Minh

School of Electrical and Electronic Engineering, Hanoi University of Science and Technology, Vietnam
tu.phamminh@hust.edu.vn-mail address

Vuong Dang Quoc

School of Electrical and Electronic Engineering, Hanoi University of Science and Technology, Vietnam
vuong.dangquoc@hust.edu.vn
(corresponding author)

Received: 2 September 2022 | Revised: 27 October 2022 | Accepted: 27 October 2022

ABSTRACT

A permanent magnet assistance synchronous reluctance motor can start directly with a net voltage or a power converter via a torque control method. However, this motor has usually a higher irreversible demagnetization level in comparison with interior permanent magnet motors, due to the fewer permanent magnets in rotor slots. In order to cope with this disadvantage, different arrangements of permanent magnets in the rotor of the line-start permanent magnet assistance synchronous reluctance motor are proposed in this paper. The V magnet shape taking skewed slots and demagnetization effect into account with the short circuit current are investigated by the finite element approach. The efficiency, torque, and output power of the proposed model have been also improved. Finally, the rotor with 3V layered magnets is prototyped to verify the efficiency of the proposed motor.

Keywords-*line start permanent magnet assistance-synchronous reluctance; magnet shape; skewed slots; demagnetization effect; finite element method*

I. INTRODUCTION

The Line Start Permanent Magnet Assistance Synchronous Reluctance Motors (LS-PMA-SynRMs) have recently been presented [1]. Authors in [2] proposed the design and optimization of low torque ripple and high torque by using ferrite magnets. However, the influences of skewed slots and the demagnetization effects on the LS-PMA-SynRMs have not been mentioned so far. In this paper, different arrangements of permanent magnets in the rotor taking skewed slots and the demagnetization effects taken into account are developed to improve the efficiency of the LS-PMA-SynRMs. Normally,

when the LS-PMA-SynRMs are operated at synchronous speed, the secondary copper loss is eliminated, leading to efficiency improvement. Less use of rare-earth materials, low cost, comparable constant-power speed range, maximum torque, and the efficiency of the LS-PMA-SynRMs will be considered. In particular, this is an interesting choice for the application of electric traction because it has a special flux barrier and suitable magnet arrangement to improve the constant torque in a wide speed range. In addition, it has a lesser risk of irreversible demagnetization in the short circuit and overheat temperature [3].

II. MODEL OF LS-PMA-SYNRMS

A 7.5kW LS-PMA-SynRM model for 6 poles is shown in Figure 1. The stator has 36 slots and the 3-layer rotor has 36 round bars. The magnetic material and silicon steels are made in N38UH and 35A350. The response of magnets to the demagnetizing influence is considered in this research. Depending on the type of magnets, the motor can either need to withstand irreversible demagnetization during a transient short circuit fault condition or only require that the demagnetization is avoided during the steady-state operating conditions. For the sintered NdFeB and SmCo magnets, an irreversible demagnetization will occur at the very high temperature of 120°C. On the other hand, the irreversible demagnetization will occur at low temperatures (i.e. below 0°C) for the sintered ferrite magnets. Initially, a temperature value can be fixed to investigate the possible demagnetization. For example, it will be assumed that the magnet temperature is 160°C. Hence, for a selected N38UH magnet, the knee point of the demagnetization curve at the specified temperature is indicated in Figure 2 [4]. It can be seen that the flux density of the B-H curve becomes non-linear. The irreversible demagnetization in the magnet will appear if the flux density is depressed below that point. It should be noted the curve becomes non-linear at about 0.2T – at 160°C (the magnet temperature of our model). When the knee point is higher, then the magnet is more easily irreversibly demagnetized at high temperatures.

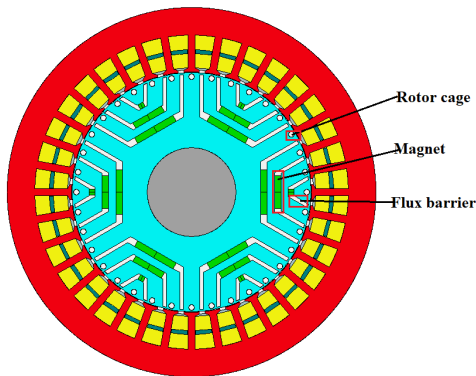


Fig. 1. LS-PMA-SynRM with 3V layer.

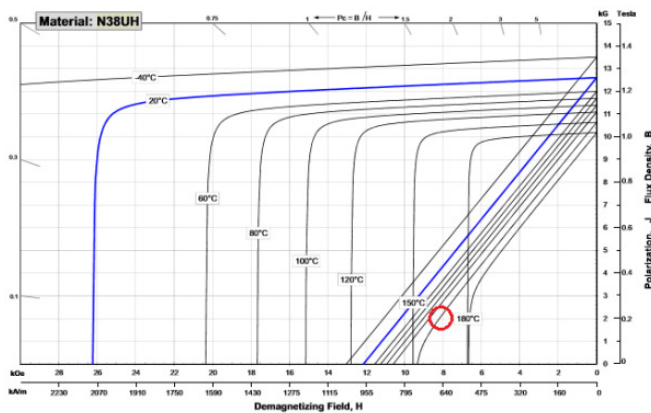


Fig. 2. Magnetization curve of B-H.

The magnetization curve with a higher temperature is pointed out in Figure 3 [4]. The curve of irreversible demagnetization is described by [5-7]:

$$B = B_r + \mu_0 \mu_r H_c - E \cdot e^{-k_1(k_2 + H_c)} \tag{1}$$

where B is the flux density, B_r is the remanent flux density, H_c is the coercivity, E is the electrical field, and k_1 and k_2 are respectively the factors of the magnets, where the factor k_2 can be defined as [8, 9]:

$$k_2 = \frac{\ln[(B_r + (\mu_r - 1)\mu_0 H_c) \frac{1}{E}]}{k_1} - H_c \tag{2}$$

The working point of the magnet is defined by the intersection between the flux density (B_m) and magnetic field strength (H_m). A point on the demagnetization characteristic of the magnet and load line is also defined. The slope of the load line is called the permeance coefficient. It is determined principally by the ratio of the magnet length to the air gap (g). When the machine is under load, the whole load line shifts, usually to the left, so the working point is shifted further down the curve. Once it overcomes the knee of the curve, an irreversible loss of magnetization will appear. Via the computation of demagnetization, it is certain that the operating point of the magnet stays above the knee. It also needs to be ensured that the magnet is working with the worst-case parameters. In particular, temperature is critical. For high-energy magnets, when the temperature increases, both B_r and H_c decrease. However, the knee moves to a lower value of H_m , which means that less current is required to demagnetize the magnet. The maximum current that can flow and its phase angle must also be considered. Normally, the current is regulated by the inverter unit, thus the maximum current is tightly controlled. But there may be fault conditions where the current reaches a value much higher than normal.

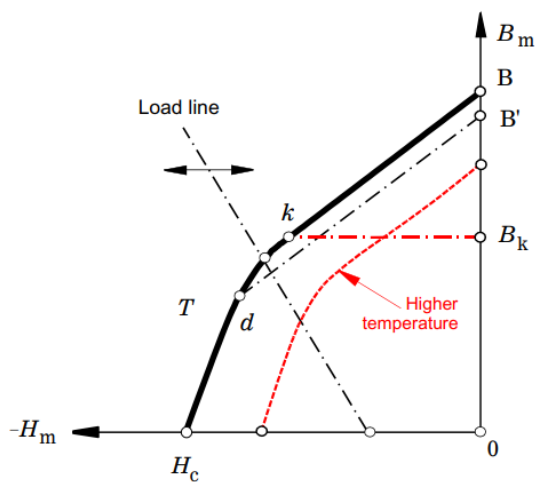


Fig. 3. B-H magnetization curve with higher temperature.

In the worst conditions, for a three-phase short-circuit, the temperature of the magnet is 250°C. For that, the current can be presented as [4]:

$$I_{d[sc]} = \frac{E_{q1}}{X_d} \tag{3}$$

where E_{q1} is the Root Mean Square (RMS) of the Electromotive Force (EMF) per phase and X_d is the d -axis synchronous reactance. Normally, this current is 2 to 5 times the maximum working current. The design parameters of LS-PMA-SynRM are given in Table I.

The schematic diagram of the proposed PMA-SynRM machine is presented in Figure 4. In the proposed motor, the magnet shape is arranged with the U-shape. This arrangement is regarded as requisite for the efficient operation in the type of I-W-U shape. The total weight of the magnet segment and copper winding is presented in Table II.

TABLE I. GEOMETRY PARAMETERS OF LS- PMA-SYNRM

Parameter	Values	Unit
Slot number	36	slot
Outer stator	210	mm
Inner stator	132	mm
Tooth width	5	mm
Slot depth	19	mm
Motor length	180	mm
Stator Lam length	180	mm
Magnet length	150	mm
Magnet size	5×2	mm
Air gap	0.4	mm
Turn per coil	20	turn

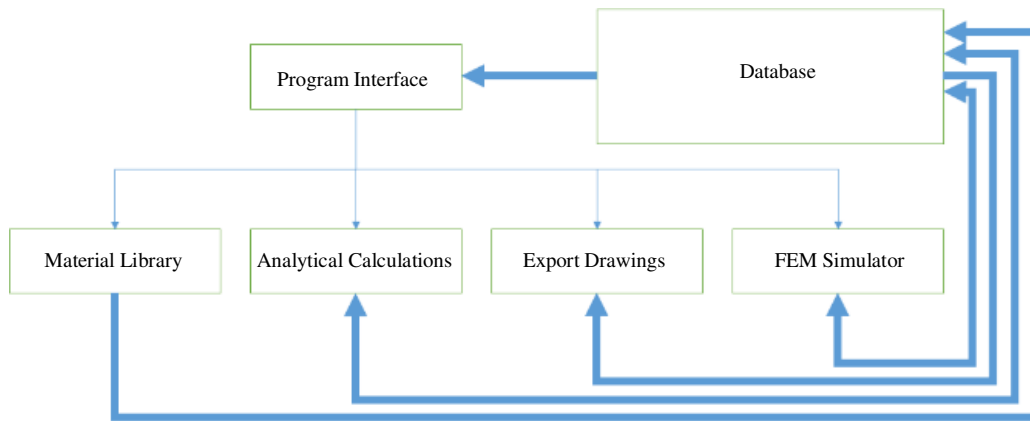


Fig. 4. Schematice driagram.

TABLE II. WEIGHT OF LS- PMA-SYNRM

Parameter	Kg
Stator lam (back iron)	8.26
Stator Lam (yooth)	5.245
Stator lamination (total)	13.5
Armature winding (active)	4.138
Armature EWdg (front)	1.027
Armature EWdg (rear)	1.027
Armature winding (total)	6.193
Rotor lam (back iron)	5.37
IPM magnet pole	4.833
Rotor lamination (total)	10.74
Magnet	0.5
Total	33.98

$$T_{EM} = \frac{3p}{2} [\lambda_{pm} \cdot i_d + (L_d - L_q) \cdot i_d \cdot i_q] \tag{4}$$

$$L_d = \frac{\lambda_d - \lambda_{pm}}{i_d} \Big|_{i_d = 0} \tag{5}$$

$$L_q = \frac{\lambda_q}{i_q} \Big|_{i_q = 0} \tag{6}$$

where λ_{pm} is the flux linkage generated by the PM field, i_d and i_q are respectively the direct and quadrature axis currents, and L_d and L_q are the direct and quadrature axis inductances. The term λ_{pm} depends on magnet sizes. The terms (L_d and L_q) are computed following to the rotor magnet barrier and magnet pole U shape.

III. LS-PMA-SYNRM PERFORMANCE IN DIRECT START AND TRACTION

The proposed PMA-SynRM machine was designed and analyzed in traction. The electromagnetic torque is formed from two components of magnetic reluctance torques. The Permanent Magnet (PM) component is produced via the interaction between the air-gap magnetic field and the armature reaction magnetic field. The reluctance component is instead based on the asymmetry between the magnetic circuit of d -axis and q -axis. The electromagnetic torque can then be defined as [5-9]:

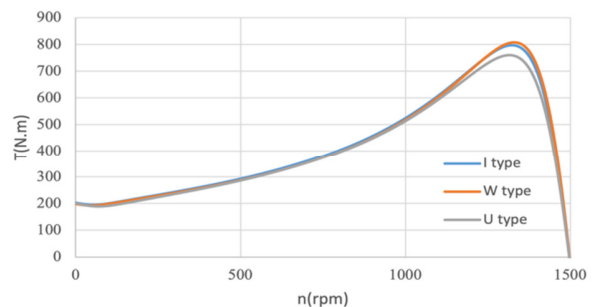


Fig. 5. Comparison of dynamic starting torque and speed with different types of I-W-U.

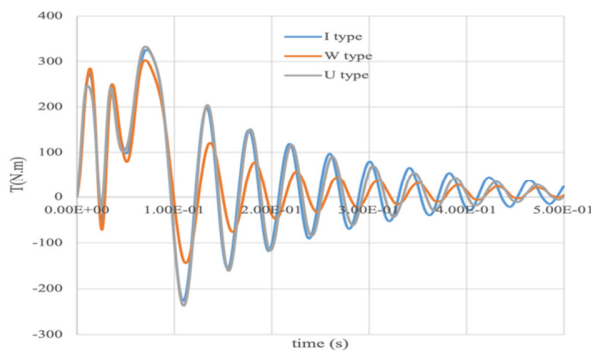


Fig. 6. Comparison of dynamic starting torque and time with different types of I-W-U.

The dynamic starting torque and speed with different types of I-W-U are shown in Figures 5 and 6. For the U-shape, the peak torque has been verified at 1500rpm. When increasing the phase current density up to 10A/mm², the peak torque is 340Nm. It should be noted that the LS-PMA-SynRM can be pre-determined by 11kW under the direct start. If this motor is operated with the power inverter, the maximum power is doubled, and the peak torque is about 800Nm (Figure 5). The parameter comparison of the LS-PMA-SynRM with different types of I-W-U is given in Table III.

TABLE III. PARAMETER COMPARISON OF LS-PMA-SYNRM

Parameters	I shape	W shape	U shape	Unit
Shaft torque	53.67	54.267	55.667	Nm
Input power	9123.3	9213.4	9273.3	W
Output power	8644.1	8474.3	8744.1	W
Total losses	519.5	522.1	529.15	W
System efficiency	93.24	94.3	94.68	%
Armature DC copper loss	340	340	340	W
Magnet loss	178.8	168.3	168	W
Stator iron loss	10.33	10.33	10.33	W
Phase terminal voltage	289.1	289.1	289.1	V
Harmonic distortion line-line terminal voltage	4.89	4.289	3.089	V
Harmonic distortion phase terminal voltage	13.7	12.2	11.27	%
Back EMF line-line voltage	111	112	114	%

TABLE IV. TEMPERATURE OF LS-PMA-SYNRM

No	Component	T (°C)
1	T (ambient)	40
2	T (housing - active)	78.717
3	T [stator lam (back iron)]	84.833
4	T (stator surface)	88.403
5	T (rotor surface)	88.65
6	T (airgap banding)	88.651
7	T (magnet)	88.197
8	T (airgap banding)	88.651
9	T (rotor lamination)	88.674
10	T (shaft - center)	87.375
13	T (active winding minimum)	87.352

It can be seen that the maximum efficiency is 94%. The total loss errors between the three cases are smaller than 5%. For the errors on the harmonic distortion line, they are lower than 14%. The temperatures of the LS-PMA-SynRM are presented in Table IV. The maximum temperature of the

winding is 90.7°C, which is much lower than isolation class H (180°). The temperature of the magnet is 88.17°C. The dynamic starting torque and speed of the U shape is shown in Figure 7. The output power of the U shape is indicated in Figure 8. The map distribution of the rotor temperature with the U shape is shown in Figure 9. The maximum temperature is 88.7°C.

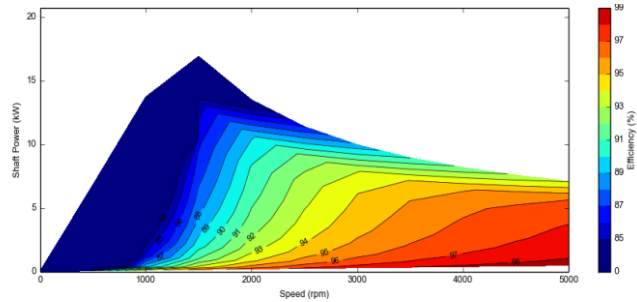


Fig. 7. Dynamic starting torque and speed of U shape design.

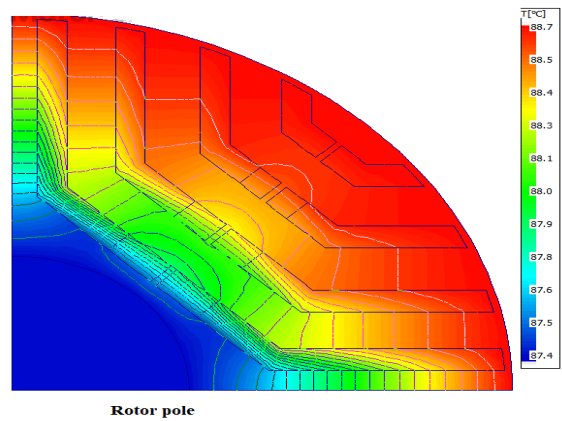


Fig. 8. Output power and speed map of the U shape.

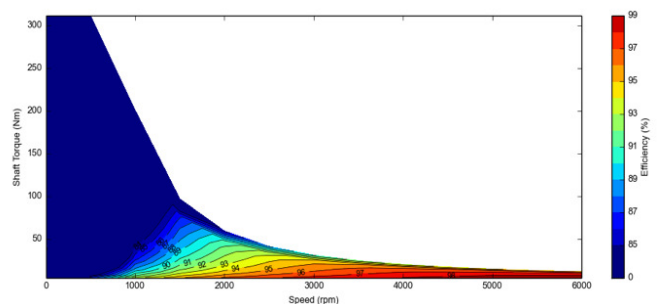


Fig. 9. Rotor temperature with the U shape.

IV. CONCLUSION

In this paper, the influence of skewed slots and demagnetization effects on the LS PMA-SynRM has been successfully investigated and analyzed. The values of dynamic starting torque and speed with different types of I-W-U have been also compared. The obtained results have shown that for the U shape, the torque and power density are noticeable improved, and the volume of magnets is the lowest. For a short starting time, the speed is considered as a constant in

comparison with the I and W shapes. The validation of the selected machine in the traction application and the full map of dynamic starting torque and power have been presented. In particular, the comparison of efficiency performances have been investigated with three different shapes, i.e. I, W, and U. Thermal simulation is also implemented to validate overheat capacity.

ACKNOWLEDGEMENT

This study was funded by the University of Transport and Communications, Hanoi, Vietnam under grant number T2022-DT-005.

REFERENCES

- [1] H. Kim *et al.*, "Study on Analysis Method of Asymmetric Permanent Magnet Assistance Synchronous Reluctance Motor Considering Magnetic Neutral Plane Shift," *IEEE Transactions on Applied Superconductivity*, vol. 30, no. 4, pp. 1–4, Jun. 2020, <https://doi.org/10.1109/TASC.2020.2968012>.
- [2] C. Gong and F. Deng, "Design and Optimization of a Low-Torque-Ripple High-Torque-Density Vernier Machine Using Ferrite Magnets for Low-Speed Direct-Drive Applications," in *2021 IEEE International Electric Machines & Drives Conference (IEMDC)*, Feb. 2021, pp. 1–8, <https://doi.org/10.1109/IEMDC47953.2021.9449586>.
- [3] D. B. Minh, N. H. Phuong, V. D. Quoc, and H. B. Duc, "Electromagnetic and Thermal Analysis of Interior Permanent Magnet Motors Using Filled Slots and Hairpin Windings," *Engineering, Technology & Applied Science Research*, vol. 12, no. 1, pp. 8164–8167, Feb. 2022, <https://doi.org/10.48084/etasr.4683>.
- [4] M. Olszewski, "Oak Ridge National Laboratory Annual Progress Report for the Power Electronics and Electric Machinery Program," Oak Ridge National Laboratory, Oak Ridge, TN, USA, ORNL/TM-2011/263, Oct. 2011.
- [5] X. Chen, J. Wang, B. Sen, P. Lazari, and T. Sun, "A High-Fidelity and Computationally Efficient Model for Interior Permanent-Magnet Machines Considering the Magnetic Saturation, Spatial Harmonics, and Iron Loss Effect," *IEEE Transactions on Industrial Electronics*, vol. 62, no. 7, pp. 4044–4055, Jul. 2015, <https://doi.org/10.1109/TIE.2014.2388200>.
- [6] D. B. Minh, L. D. Hai, T. L. Anh, and V. D. Quoc, "Electromagnetic Torque Analysis of SRM 12/8 by Rotor/Stator Pole Angle," *Engineering, Technology & Applied Science Research*, vol. 11, no. 3, pp. 7187–7190, Jun. 2021, <https://doi.org/10.48084/etasr.4168>.
- [7] D. B. Minh, V. D. Quoc, and P. N. Huy, "Efficiency Improvement of Permanent Magnet BLDC Motors for Electric Vehicles," *Engineering, Technology & Applied Science Research*, vol. 11, no. 5, pp. 7615–7618, Oct. 2021, <https://doi.org/10.48084/etasr.4367>.
- [8] M. Taniguchi *et al.*, "Development of New Hybrid Transaxle for Compact-Class Vehicles," SAE International, Warrendale, PA, USA, SAE Technical Paper 2016-01-1163, Apr. 2016, <https://doi.org/10.4271/2016-01-1163>.
- [9] Y. Wang, N. Bianchi, and R. Qu, "Comparative Study of Non-Rare-Earth and Rare-Earth PM Motors for EV Applications," *Energies*, vol. 15, no. 8, Jan. 2022, Art. no. 2711, <https://doi.org/10.3390/en15082711>.